PHYSICAL MODELS AND REFINED ORBITS FOR ASTEROIDS FROM GAIA PHOTOMETRY AND ASTROMETRY

Mikko Kaasalainen[1], **Daniel Hestroffer**[2], **Paolo Tanga**[3]

[1]Department of Mathematics and Statistics, Rolf Nevanlinna Institute,
University of Helsinki, PO Box 4, FIN-00014 Helsinki, Finland
[2]Observatoire de Paris, IMCCE / CNRS UMR 8028, 77 Av. Denfert Rochereau, 75014 Paris, France
[3]Observatoire de la Côte d'Azur, Cassiopée, CNRS UMR 6202, Le Mont Gros, BP 4229, 06304 Nice cedex 4, France

ABSTRACT

Gaia will make accurate photometric and astrometric observations of thousands of asteroids in sparse epoch sequences. We show that sparse photometric data are usually sufficient for obtaining the sidereal period, the pole direction, and a coarse estimate of the global shape (or binary character) of the target. Some light-scattering characteristics (solar phase function for the Gaia phase angle range) are also obtained. Furthermore, we show that the photocentre offset effect of ultraprecise astrometry can be efficiently combined with photometric data sets to yield improved physical models of asteroids. This is done by solving the full inverse problem for the target's orbit, size, shape, spin state, and scattering properties. The shape and the spin state of the target are more accurate than from photometry alone, and the barycentre residuals for the orbit are considerably smaller than those from uncorrected (or crudely corrected) astrometric measurements. This scheme also removes the double-pole ambiguity of photometrically derived spin states of targets close to the plane of the ecliptic.

Key words: Gaia; Solar System; Minor planets; Photometry; Astrometry; Numerical methods.

1. INTRODUCTION

During its mission, Gaia will observe thousands of asteroids in sparse but well-distributed time sequences. A typical number of accurate brightness measurements for one asteroid's sequence is between 50 and 100. In Kaasalainen (2004), it was shown that such a sequence is sufficient for revealing the basic physical characteristics of the target, and that such sequences can be obtained with both ground-based and satellite-platform calibrated photometric surveys.

While photometric observations form a stable modelling basis by providing a global-scale physical model of the target (Kaasalainen et al. 2001), complementary data can efficiently be used to refine this model. Indeed, multi-datainversion, i.e., using all available data simultaneously for constructing a model of the target, has become an important concept particularly for small Solar System objects. For example, even one good Doppler radar profile can resolve non-convex details for a photometrically well-observed target (Kaasalainen 2003). Other such sources are, e.g., interferometry, adaptive optics snapshots, and occultation timings.

An obvious way of giving further boost to the sparse-set photometric modelling prospect is to add complementary data to the data set with, e.g., a few additional detailed lightcurves, radar scans, or snapshots. In connection with Gaia, a convenient option of obtaining complementary data is automatically provided by the astrometric observations. The characteristics of the astrometric photocentre-barycentre offset effect for asteroids were discussed in Kaasalainen & Tanga (2004), where we also noted that this effect alone is not sufficient for providing information for asteroid modelling. Here we will show that, combined with sparse photometric data, the photocentre offset is a useful source of information in the inverse problem.

2. INVERSION OF SPARSE PHOTOMETRY

Photometric sequences can directly be analyzed with the general technique of Kaasalainen et al. (2001), where we minimize the photometric chi-square residual $\chi^2_{\rm pm}$ comprising the observed and modelled brightnesses $L_i, L(t_i)$:

$$\chi^2_{\rm pm} = \sum_{i=1}^{N} [L(t_i) - L_i]^2 \qquad (1)$$

If the calibration accuracy of L_i is at least about 0.05 mag, the procedure finds the global minimum and converges very robustly (Kaasalainen 2004). The best sidereal period of the target peaks quite strongly in the initial search (Figure 1), after which the pole and shape can be refined to obtain the best fit (Figure 2). This performance

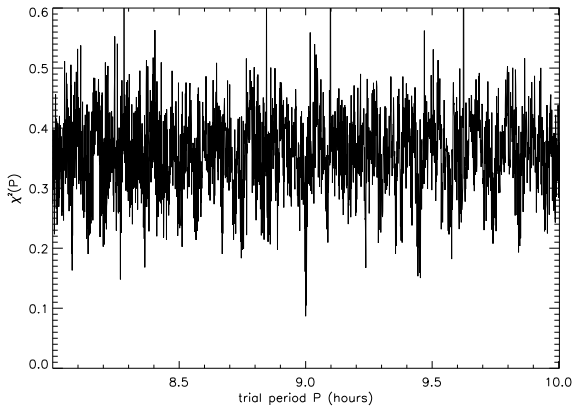

Figure 1. Chi-square as a function of initial period guess for simulated Gaia data for an MBA-target. The correct period of 9 h clearly stands apart.

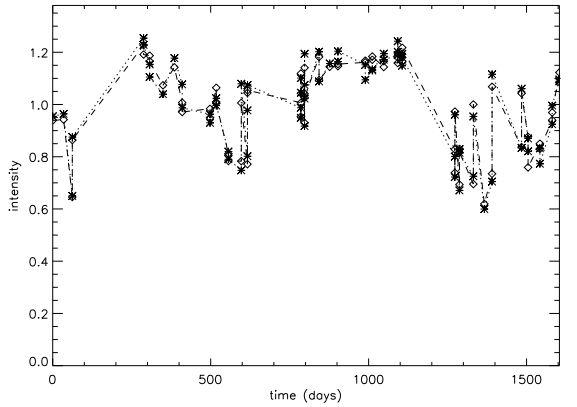

Figure 2. Simulated observations (asterisks and dotted line) and the best model fit (diamonds and dashed line) for the MBA-case; photometric noise and fit rms deviation are both 0.03 mag.

is possible because the underlying physical model introduces strict consistency constraints, i.e., we have much more information than if we treated the time sequence without physical modelling as in standard time series analysis. This requires good temporal coverage: observations over several years should find the target in various observing geometries. The light-scattering behaviour of the object can typically be modelled with the exponential-linear solar phase function (Kaasalainen et al. 2001) particularly as Gaia observations tend to be in the linearly dominated solar phase range (with the slope as a free parameter).

3. INVERSION OF COMBINED SPARSE PHOTOMETRY AND ASTROMETRY

In addition to refining photometry-based models, ultra-precise astrometry can be used to solve for the object's size and orbit, and for removing the common photometric $\pm 180°$–ambiguity in the ecliptic longitude of the pole direction for asteroids moving close to the plane of the ecliptic.

The astrometric photocentre offset is closely related to the disc-integrated brightness L of the target. In the object's own coordinate system, the photocentre is defined by

$$\mathbf{x}_{\rm pc} = \frac{1}{L}\int_A \mathbf{x}\, dL \qquad (2)$$

where the integration region A is over the illuminated and visible parts of the surface, and a surface patch at $\mathbf{x}$ contributes the amount dL to the observed total brightness. The plane-of-sky (POS) projection of $\mathbf{x}_{\rm pc}$ depends on the target's rotation parameters and the observing geometry (Kaasalainen & Tanga 2004).

The inverse solution is found by minimizing the objective function

$$\chi^2 = \chi^2_{\rm pm} + \Lambda\chi^2_{\rm pc} \qquad (3)$$

where Λ is a suitable weight factor for the astrometric part $\chi^2_{\rm pc}$ which is a function of POS projections of the orbit and the photocentre offset as given in Kaasalainen & Tanga (2004):

$$\chi^2_{\rm pc} = \sum_{i=1}^{N}[\cos^2\delta_i\,(\alpha_{\rm pc}(t_i)-\alpha_i)^2 + (\delta_{\rm pc}(t_i)-\delta_i)^2] \quad (4)$$

where (α_i, δ_i) and $(\alpha_{\rm pc}(t_i), \delta_{\rm pc}(t_i))$ are, respectively, the observed and the modelled photocentre POS positions. The epoch sequences t_i, $i = 1, ..., N$ for the astrometric and photometric points are taken to be the same in the example presented here, but this choice is irrelevant.

Since the photocentre effect is extremely small, of order milliarcseconds (mas), the POS positions are best defined and computed by using a fixed nearby reference orbit (given by suitable corresponding orbital parameters) and its corresponding POS projections at epochs t_i. Such a reference orbit is given by, e.g., the usual best-fit (osculating) orbit solution directly from (α_i, δ_i) (here we assume that all the observations can be attributed to the correct object; the linking problem particularly for previously unknown projects is a separate subject studied elsewehere). Here we take the six orbit parameters to be the Cartesian position and velocity coordinates at some initial epoch t_0, and all osculating effects are directly introduced through the perturbing forces in the integration of the equations of motion. Thus the orbit parameters of the reference orbit are the six constants $(\mathbf{r}_0, \mathbf{v}_0) = (\mathbf{r}(t_0), \mathbf{v}(t_0))$, and the orbit is the function $\mathbf{r}(t) = \mathbf{r}(\mathbf{r}_0, \mathbf{v}_0, t)$. The nearby orbits $\mathbf{r}'(t) = \mathbf{r}(\mathbf{r}_0 + \Delta\mathbf{r}_0, \mathbf{v}_0 + \Delta\mathbf{v}_0, t)$ are given by the difference $\Delta\mathbf{r} = \mathbf{r}' - \mathbf{r}$ through the transition matrix:

$$\Delta\mathbf{r}(t) = \frac{\partial\mathbf{r}(t)}{\partial(\mathbf{r}_0, \mathbf{v}_0)}\begin{pmatrix}\Delta\mathbf{r}_0\\ \Delta\mathbf{v}_0\end{pmatrix} \qquad (5)$$

The corresponding POS position changes by

$$\begin{pmatrix}\Delta\alpha(t)\\ \Delta\delta(t)\end{pmatrix} = \frac{\partial}{\partial\mathbf{r}}(\alpha[\mathbf{r}(t), \mathbf{r}_\oplus(t)], \delta[\mathbf{r}(t), \mathbf{r}_\oplus(t)])\Delta\mathbf{r}(t) \qquad (6)$$

where $\mathbf{r}_\oplus$ is the position of the observer. Thus the orbit parameters to be solved for in the inverse problem are the initial deviations $(\Delta\mathbf{r}_0, \Delta\mathbf{v}_0)$ from the adopted

reference orbit (and (α, δ) in the square terms of Equation 4 can be replaced by $(\Delta\alpha, \Delta\delta)$). For accurate orbit integration to be used in the eventual Gaia analysis, the transition matrix for the reference orbit can be obtained simultaneously with the integrated $\mathbf{r}$. In addition to the six initial phase-space coordinates, further adjustable parameters such as the masses of perturbing bodies can be introduced through the orbit integration by using additional partial derivatives of $\mathbf{r}(t)$. For the example in this paper, we use just the two-body Kepler orbit as this does not change the conclusions. Thus the transition matrix reads here

$$\frac{\partial \mathbf{r}(t)}{\partial \mathbf{r}_0} = f(t)\mathsf{I} + \mathbf{r}_0 \otimes \frac{\partial f(t)}{\partial \mathbf{r}_0} + \mathbf{v}_0 \otimes \frac{\partial g(t)}{\partial \mathbf{r}_0} \quad (7)$$

$$\frac{\partial \mathbf{r}(t)}{\partial \mathbf{v}_0} = g(t)\mathsf{I} + \mathbf{r}_0 \otimes \frac{\partial f(t)}{\partial \mathbf{v}_0} + \mathbf{v}_0 \otimes \frac{\partial g(t)}{\partial \mathbf{v}_0} \quad (8)$$

with the reference orbit given by Gauss' f, g-functions (see Danby 1987; Kaasalainen & Laakso 2001) as $\mathbf{r}(t) = f(\mathbf{r}_0, \mathbf{v}_0, t)\mathbf{r}_0 + g(\mathbf{r}_0, \mathbf{v}_0, t)\mathbf{v}_0$, I is the identity matrix, and the outer product is defined by $(\mathbf{a} \otimes \mathbf{b})_{ij} \equiv a_i b_j$.

We show the POS photocentre plots such that the origin of the plot is comoving with the reference orbit POS location. The photocentre observations (pluses) are thus the full deviations from this orbit. The corresponding model points (asterisks) are rendered as the *residuals* between the observed and modelled points as in Kaasalainen & Tanga (2004), so the tighter the asterisk group around the origin, the better the model fit. In Figure 3, we first show this plot for the photometric inverse spin/shape solution of the main-belt asteroid (MBA) Gaia example of Figures 1 and 2. Only the size of the shape solution has been optimized here (as it is not included in the photometric inverse problem). The target (a Gaspra-like body in a Vesta-like orbit) was chosen to be 180 km wide across its largest dimension, with the pole direction at the ecliptic longitude and latitude $(\lambda, \beta) = (90°, 90°)$, and sidereal rotation period $P = 9$ hours. (As shown in Kaasalainen & Tanga (2004), all realistic scattering models produce virtually the same photocentre locations within the practical astrometric accuracy for asteroids.) The pole obtained in photometric inversion of the 69 Gaia data points is at $(\lambda, \beta) = (92°, 101°)$ with $P = 9.00001$ h. The photocentre offset scatter is reduced somewhat in $\Delta\alpha$-direction, but the result is obviously not as good as for a model from a large photometric data base as shown in Kaasalainen & Tanga (2004). This indicates that it would be useful to improve the model by fitting astrometry and photometry simultaneously.

We assume here that the initial guesses for the combined astrometry and photometric inverse problem are the solutions of the separate problems as above and can be expected to be already in the global minimum area of the parameter space, so no global parameter scanning grid is needed. In any case, such a grid is readily implemented whenever necessary, so we do not comment further on this aspect here.

The objective function is minimized as in Kaasalainen et al. (2001) by using the Levenberg–Marquardt algorithm and a function series for the radii of the shape model. A sphere is usually the best choice for an initial

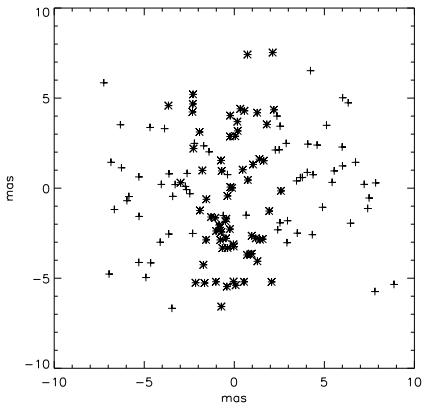

Figure 3. Photocentre observations (pluses) and the residuals (asterisks) of the modelled photocentre locations for the shape/spin model from photometric Gaia data only.

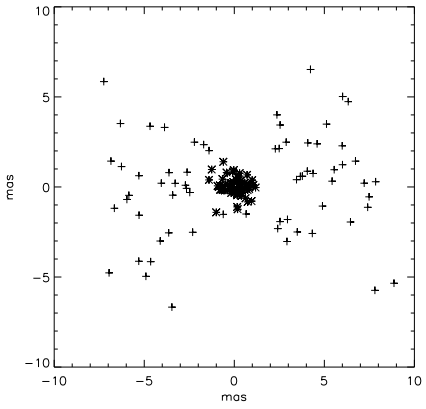

Figure 4. Photocentre observations (pluses) and the residuals (asterisks) of the modelled photocentre locations for the shape/spin and orbit model from combined astrometric and photometric Gaia data.

shape. The only additional parameters are now the initial orbit values $(\Delta\mathbf{r}_0, \Delta\mathbf{v}_0)$. The result is shown in Figure 4: the residuals are now much smaller and the shape solution in Figure 5 looks basically similar to the original one in Figure 6, with corresponding dimensions – a remarkable result as we use only 69 epochs. The improved pole position is at $(\lambda, \beta) = (90°, 93°)$ with $P = 9.0000003$ h, and the position and velocity deviations from the correct values are (0.68 km, 5.48 km, -0.74 km) and (-0.27 mm/s, 0.05 mm/s, 0.01 mm/s). The accuracies of the latter are, of course, due to the idealized knowledge of orbital physics, but they serve to illustrate the robust orbit convergence properties as the corresponding residual scatter due to the orbit solution is less than 1 mas.

The model photocentres thus fit the observed ones practically down to the astrometric inaccuracy level. Any tighter astrometric residuals can be obtained only at the expense of fast decreasing goodness of the photometric fit. The best results seem to be obtained by letting the photometric χ^2_{pm} get some 10%−20% larger than the value at $\Lambda = 0$.

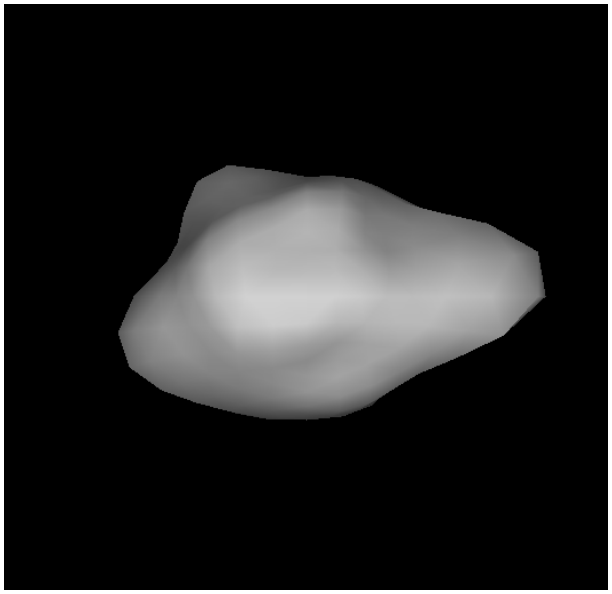

Figure 5. The shape solution for the combined photometric and astrometric inverse problem, obtained with only 69 epochs.

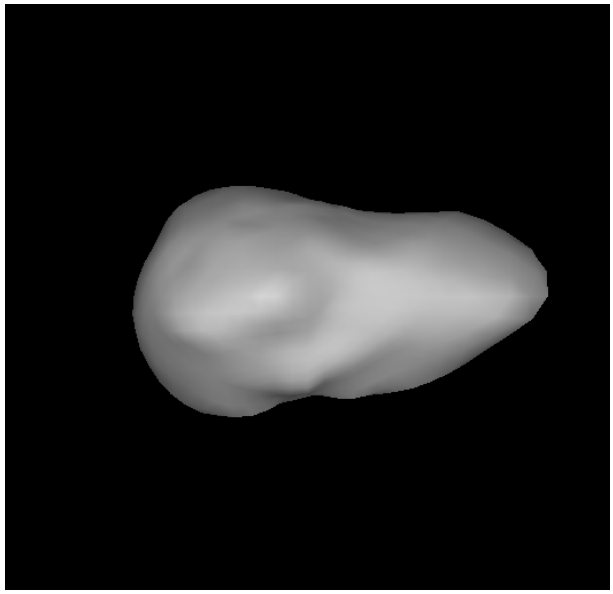

Figure 6. Image of the original shape.

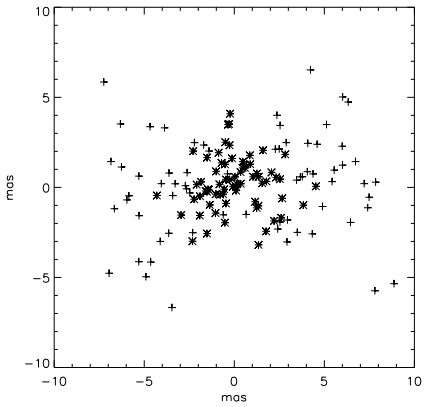

Figure 7. Photocentre observations (pluses) and the residuals (asterisks) of the modelled photocentre locations for the wrong 180°-shifted pole.

The only parameter that may have a poorly defined initial value is the size, so the expected size range may have a number of local χ^2–minima. An initial size scan is required with at least some 10% intervals, usually meaning a few guesses.

Our example also establishes the scaling properties of the inverse problem: typically astrometric accuracy of order 1% of the apparent diameter of the target is needed to fully exploit astrometric data in the multidatainversion scheme. Thus astrometric photocentre accuracy of 1 mas is typically sufficient for this kind of modelling for targets with apparent diameter of roughly 100 mas, and 0.1 mas accuracy would already reach 10 mas–diameter class. Due to asteroids' motion, their astrometric accuracy levels cannot be expected to be as good as for stellar objects, but 1 mas is expected to be generally reachable and even 0.1 mas should be possible in some cases (Hestroffer & Berthier 2005).

In addition to size ambiguity, photometric inversion often cannot properly distinguish between two pole solutions some 180° apart in ecliptic longitude if the target is close to the plane of the ecliptic. Astrometric data have the important possibility to remove this ambiguity as the mirror shape solutions for the mirror poles have quite different POS projections even though their disc-integrated brightnesses were the same. Thus the residuals for the wrong pole are clearly larger (Figure 7).

4. CONCLUSIONS

Gaia photometry is usually sufficient for basic asteroid modelling, and its combination with high-precision astrometric data in a full inverse problem can be used for more accurate modelling via the photocentre offset effect. We also get a size scale for the shape solution. This mode requires accurate modelling of orbits, so the masses of perturbing asteroids need to be solved for in addition to the initial orbital parameters. We are now investigating whether 'tougher' cases such as binary asteroids are distinguishable from sequences contaminated by outliers and can be modelled as robustly as 'ordinary' targets.

REFERENCES

Danby, J.M.A. 1987, Fundamentals of Celestial Mechanics (Richmond: Willman-Bell)

Hestroffer, D., Berthier, J., 2005, ESA SP-576, this volume

Kaasalainen, M., Torppa, J., Muinonen, K. 2001, Icarus, 153, 37

Kaasalainen, M. & Laakso, J. 2001, A&A, 368, 706

Kaasalainen, M. 2003, JRASC, 97, 283

Kaasalainen, M. & Tanga, P. 2004, A&A, 416, 367

Kaasalainen, M. 2004, A&A, 422, L39